

Polarization Ellipse Analysis of Nonstationary Random Signals

Peter J. Schreier, *Member, IEEE*

Abstract—We present a novel way of extending rotary-component and polarization analysis to nonstationary random signals. If a complex signal is resolved into counterclockwise and clockwise rotating phasors at one particular frequency only, it traces out an ellipse in the complex plane. Rotary-component analysis characterizes this ellipse in terms of its shape and orientation. Polarization analysis looks at the coherence between counterclockwise and clockwise rotating phasors and whether there is a preferred rotation direction of the ellipse (counterclockwise or clockwise). In the nonstationary case, we replace this ellipse with a time-dependent local ellipse that, at a given time instant, gives the best local approximation of the signal from a given frequency component. This local ellipse is then analyzed in terms of its shape, orientation, and degree of polarization. A time-frequency coherence measures how well the local ellipse approximates the signal. The ellipse parameters and the time-frequency coherence can be expressed in terms of the Rihaczek time-frequency distribution. Under coordinate rotation, the ellipse shape, the degree of polarization, and the time-frequency coherence are invariant, and the ellipse orientation is covariant. The methods presented in this paper provide an alternative to ellipse decompositions based on wavelet ridge analysis.

Index Terms—Improper complex random signal, nonstationary signal, polarization analysis, Rihaczek spectrum, rotary-spectrum analysis, wavelet ridge analysis, widely linear transformation.

I. INTRODUCTION

ROTARY-SPECTRUM and polarization analysis are widely used in a number of research areas, including optics [1]–[3], geophysics [4], [5], meteorology, oceanography [6]–[8], and radar [9]. These techniques were originally developed for stationary signals. Their starting point is the Cramér–Loève spectral representation [10] for a complex harmonizable random process

$$s(t) = \int_0^{\infty} dS(f)e^{j2\pi ft} + dS(-f)e^{-j2\pi ft} \quad (1)$$

which synthesizes the random process $s(t)$ from counterclockwise turning phasors $dS(f)e^{j2\pi ft}$ and clockwise turning phasors $dS(-f)e^{-j2\pi ft}$. The contributions from counterclockwise

and clockwise rotating components at fixed frequency f describe a random ellipse

$$u_f(t) = dS(f)e^{j2\pi ft} + dS(-f)e^{-j2\pi ft} \quad (2)$$

in the complex plane. This ellipse can be characterized in terms of its shape and orientation. In oceanography, this type of analysis is referred to as the *rotary-component method* [6], [7], and has proven powerful in the interpretation of ocean current spectra [8]. It is also of interest to characterize the coherence between counterclockwise and clockwise rotating phasors. If there is complete coherence, $u_f(t)$ is said to be *completely polarized*. In optics, *polarization analysis* is employed in the study of partially coherent light [1]–[3], and the ellipse $u_f(t)$ is referred to as the *polarization ellipse*. Polarization analysis is also successfully used in geophysics [4], [5] and radar [9].

However, just as classical Fourier analysis is not adequate to deal with nonstationary signals, the classical rotary-component and polarization analysis techniques are not designed to handle nonstationarity. It is obviously impossible for a *stationary* ellipse $u_f(t)$ to capture the time-varying nature of a *nonstationary* signal $s(t)$. Previous extensions of rotary-component and polarization analysis to nonstationary signals have been centered mainly around the wavelet transform (see, e.g., [11]–[15]) and, to a lesser extent, the Short Time Fourier Transform (STFT) [15]. In the recent development [12], a nonstationary signal is approximated locally at time t by an ellipse whose parameters depend on t . The ellipse parameters are determined by wavelet ridge analysis [16], which is a technique for estimating the instantaneous frequency of a nonstationary signal.

In this paper, we present an alternative approach based on the Rihaczek time-frequency distribution (R-TFD) [17], which is a bilinear TFD contained in Cohen's class [18]. The advantage of the R-TFD is that it presents an *inner product* between the time-domain signal at given time t and its frequency-domain representation at given frequency f [19]. As such, it determines the time-varying Wiener (linear minimum mean-squared error) filter for estimating the signal at time t from a phasor rotating with frequency f [19]. Similar to [12], we replace the stationary ellipse $u_f(t)$ with a local ellipse whose parameters depend on t . However, in contrast to [12], our ellipse represents the *best local* approximation of $s(t)$ from counterclockwise and clockwise rotating components at given frequency f , in the sense that it minimizes the mean-squared approximation error. This local ellipse can then be analyzed in terms of its shape, orientation, and degree of polarization, to gain insight into the statistical properties of the nonstationary signal $s(t)$. In order to measure how well the local ellipse approximates the signal at time t , we introduce a time-frequency coherence. This time-frequency coherence and

Manuscript received July 23, 2007; revised May 12, 2008. First published May 23, 2008; last published August 13, 2008 (projected). The associate editor coordinating the review of this manuscript and approving it for publication was Dr. Eran Fishler. The work of the author was supported by the Australian Research Council under Discovery Project Grant DP0664365.

The author is with the School of Electrical Engineering and Computer Science, The University of Newcastle Callaghan, NSW 2308, Australia (e-mail: peter@peter-schreier.com).

Digital Object Identifier 10.1109/TSP.2008.925961

all ellipse parameters can be expressed in terms of the R-TFD of $s(t)$, further justifying the R-TFD as a fundamental descriptor of a nonstationary time series.

Hence, it is our point of view that polarization and rotary-component analysis are about *estimating* a signal $s(t)$ in the time domain from its frequency-domain description. In the stationary case, the widely linear minimum mean-squared error (WLM MSE) estimate of $s(t)$ is the stationary ellipse $u_f(t)$ given in (2). In the nonstationary case, the WLM MSE estimate leads to a local ellipse with time-dependent parameters. Such a local ellipse may be constructed for every point (t, f) in the time-frequency plane. This raises the question of which points (and thus, local ellipses) in the t - f plane the analysis should focus on. One possible answer would be to consider the instantaneous frequency curve, which may be estimated using wavelet ridge analysis [12], [16]. Our answer is different: We focus on points in the t - f plane where the corresponding local ellipse at (t, f) provides a good approximation of the nonstationary signal $s(t)$. These are points with magnitude-squared time-frequency coherence close to 1.

Our program for this paper is as follows. In Section II, we review some background material that is required to deal with nonstationary complex random signals, including the R-TFD. In Section III, we review the rotary-component method [6], [7] for monochromatic deterministic signals and stationary random signals. In Section IV, we then extend this theory to the nonstationary case, paying special attention to the important class of analytic signals. In particular, we will see that all analytic signals are completely polarized. A surprising finding is that, while proper analytic signals are counterclockwise circularly polarized, improper analytic signals can, at least temporarily, turn in clockwise direction. Section V deals with polarization analysis for nonstationary signals, connecting the development to some results from the study of partially polarized light [1]–[3]. Finally, Section VI wraps up the discussion. Some preliminary results from this paper have also been presented at a conference [20].

II. PRELIMINARIES

In this paper, we analyze either univariate or bivariate real signals (e.g., horizontal velocity components in geophysical measurements). Bivariate signals $(x(t), y(t))$ are combined in a complex signal $s(t) = x(t) + jy(t)$. If the signal to be analyzed is univariate real, we consider its complex analytic signal $s(t) = x(t) + jH\{x(t)\}$ instead, where $H\{x(t)\}$ denotes the Hilbert transform of $x(t)$. In this section, we present some mathematical tools that are required to deal with stationary and nonstationary random signals.

A. Rihaczek Distribution

We first review the R-TFD [17] as a means to describe the second-order statistics of a nonstationary signal. It will become clear in later sections how the Rihaczek distribution provides the basis for an evocative geometric interpretation of nonstationarity.

Whenever $s(t)$ is treated as random in this paper, it is assumed to be zero-mean and harmonizable. Its Cramér–Loève spectral

representation is then given by the mean-square convergent integral [10]

$$s(t) = \int_{-\infty}^{\infty} dS(\xi) e^{j2\pi\xi t}. \quad (3)$$

For a general nonstationary random process, the increment process $dS(\xi)$ is nonorthogonal and improper [21] with (*Hermitian*) *spectral correlation* $R_{ss^*}(\nu, \xi)$, defined by

$$E \{dS(\xi + \nu)dS^*(\xi)\} = R_{ss^*}(\nu, \xi) d\nu d\xi \quad (4)$$

and *complementary spectral correlation* [22] $R_{ss}(\nu, \xi)$, defined by

$$E \{dS(\xi + \nu)dS(-\xi)\} = R_{ss}(\nu, \xi) d\nu d\xi. \quad (5)$$

This representation can require the use of Dirac delta functions in $R_{ss^*}(\nu, \xi)$ and $R_{ss}(\nu, \xi)$; in particular, in the stationary case. Note that ξ is a global frequency variable and ν is a local frequency offset. If the complementary spectral correlation vanishes, $s(t)$ is called *proper*. If $s(t)$ is stationary, the spectral correlation and complementary spectral correlation both collapse to a delta ridge along the stationary manifold $\nu = 0$,

$$R_{ss^{(*)}}(\nu, \xi) = P_{ss^{(*)}}(\xi)\delta(\nu). \quad (6)$$

Here and in the following, $(*)$ denotes optional conjugation. Conjugation produces the Hermitian quantity, and omitting conjugation produces the complementary quantity. In (6), $P_{ss^*}(\xi) \geq 0$ is the power spectral density (PSD), and the *complementary power spectral density* (C-PSD) $P_{ss}(\xi) = P_{ss}(-\xi)$ is even but generally complex.

Since $s(t)$ is harmonizable, so are its temporal correlation and complementary temporal correlation

$$\begin{aligned} r_{ss^{(*)}}(t, \tau) &= E \left\{ s(t)s^{(*)}(t - \tau) \right\} \\ &= \int_{-\infty}^{\infty} \int_{-\infty}^{\infty} R_{ss^{(*)}}(\nu, \xi) e^{j2\pi(\nu t + \xi\tau)} d\nu d\xi. \end{aligned} \quad (7)$$

In (7), t is a global time variable and τ is a local time lag. In order to obtain a characterization in terms of global time t and global frequency ξ , we either Fourier-transform the temporal correlation and complementary correlation on local τ , or inverse Fourier-transform the spectral correlation and complementary correlation on local ν . This yields the Hermitian Rihaczek time-frequency distribution (HR-TFD) [17] and the complementary Rihaczek time-frequency distribution (CR-TFD) [22]

$$\begin{aligned} V_{ss^{(*)}}(t, \xi) &= \int_{-\infty}^{\infty} r_{ss^{(*)}}(t, \tau) e^{-j2\pi\xi\tau} d\tau \\ &= \int_{-\infty}^{\infty} R_{ss^{(*)}}(\nu, \xi) e^{j2\pi\nu t} d\nu. \end{aligned} \quad (8)$$

Together, the HR-TFD and CR-TFD comprise the R-TFD.

The R-TFD is a member of Cohen's class [18], the class of bilinear TFDs that are covariant to shifts in time and frequency. It is generally complex, yet time- and frequency-marginals of the HR-TFD are nonnegative [23]. The time-marginal is the instantaneous power at time t

$$\int_{-\infty}^{\infty} V_{ss^*}(t, \xi) d\xi = r_{ss^*}(t, 0) \geq 0 \quad (9)$$

and the frequency-marginal is the *energy spectral density* (ESD) at frequency ξ

$$\int_{-\infty}^{\infty} V_{ss^*}(t, \xi) dt = R_{ss^*}(0, \xi) \geq 0. \quad (10)$$

The complementary instantaneous power and complementary ESD (C-ESD) are derived analogously by omitting conjugation. However, both are generally complex. Formally, the ESD (C-ESD) is related to the PSD (C-PSD) as $R_{ss^{(*)}}(0, \xi) d\xi = P_{ss^{(*)}}(\xi)$. It is appropriate to use the ESD in the description of nonstationary finite-energy signals and the PSD for stationary signals. Note that $P_{ss^{(*)}}(\xi) = V_{ss^{(*)}}(t, \xi)$ for all t , if $s(t)$ is stationary.

This is the right place to dispel the widespread notion that PSDs belong to stochastic signals and ESDs to deterministic signals. The difference between PSD and ESD should not be one of stochastic versus deterministic, but obviously one of physical unit: a PSD distributes power over frequency, and an ESD distributes energy over frequency. There is no compelling reason why PSDs could not be computed for deterministic signals, or ESDs for stochastic signals.

The nonnegativity of the HR-TFD marginals has lead many to interpret the HR-TFD and other TFDs in Cohen's class as energy or power distributions. As the HR-TFD itself takes on complex values, such an interpretation seems unsatisfactory because it does not work locally in the vicinity of some point (t, ξ) in the time-frequency plane. We shall not further pursue this point of view, and instead base our development on the key insight that the R-TFD is an inner product [19]. This can be seen by explicitly computing the R-TFD (8)

$$V_{ss^*}(t, \xi) d\xi = E \left\{ s(t) (dS(\xi) e^{j2\pi\xi t})^* \right\} \quad (11)$$

$$V_{ss}(t, \xi) d\xi = E \left\{ s(t) (dS^*(-\xi) e^{j2\pi\xi t})^* \right\}. \quad (12)$$

This shows that the HR-TFD is the Hilbert space inner product between the random variable $s(t)$, at fixed time instant t , and the infinitesimal stochastic Fourier generator $dS(\xi) e^{j2\pi\xi t}$, at fixed frequency ξ . The CR-TFD is the Hilbert space inner product between $s(t)$ and $dS^*(-\xi) e^{j2\pi\xi t}$. The consequences of this finding will be explored in later sections.

B. Connections Between Real and Complex Descriptions

The second-order statistics of the complex signal $s(t) = x(t) + jy(t)$ can also be described in terms of its real and imaginary parts. We now establish how a description based on $s(t)$ is related to a description based on $x(t)$ and $y(t)$. This presents a brief review of material from [21]. While this section assumes, for simplicity, that $s(t)$ is stationary, the

results generalize in a straightforward manner to the nonstationary case.

Employing the transform matrix \mathbf{T} ,

$$\mathbf{T} = \begin{bmatrix} 1 & j \\ 1 & -j \end{bmatrix}, \quad \mathbf{T}\mathbf{T}^H = \mathbf{T}^H\mathbf{T} = 2\mathbf{I} \quad (13)$$

we can construct the augmented vector

$$[s(t) \quad s^*(t)]^T = \mathbf{T} [x(t) \quad y(t)]^T \quad (14)$$

from the real and imaginary parts. The frequency-domain analog is

$$[dS(\xi) \quad dS^*(-\xi)]^T = \mathbf{T} [dX(\xi) \quad dY(\xi)]^T. \quad (15)$$

The correlation of the frequency-domain augmented vector is

$$\begin{aligned} E \begin{bmatrix} dS(\xi) \\ dS^*(-\xi) \end{bmatrix} \begin{bmatrix} dS^*(\xi) \\ dS(-\xi) \end{bmatrix}^T &= \begin{bmatrix} P_{ss^*}(\xi) & P_{ss}(\xi) \\ P_{ss^*}^*(\xi) & P_{ss^*}(-\xi) \end{bmatrix} d\xi \\ &= \mathbf{P}_{ss^*}(\xi) d\xi. \end{aligned} \quad (16)$$

We call $\mathbf{P}_{ss^*}(\xi)$ the *power spectral density (PSD) matrix*. Since $\mathbf{P}_{ss^*}(\xi)$ is positive semidefinite, we must have $P_{ss^*}(\xi) \geq 0$, $P_{ss}(\xi) = P_{ss}(-\xi)$, and $|P_{ss}(\xi)|^2 \leq P_{ss^*}(\xi)P_{ss^*}(-\xi)$. Because matrices $\mathbf{P}_{ss^*}(\xi)$ and $\mathbf{P}_{ss^*}(-\xi)$ are trivially related, it is sufficient to consider $\mathbf{P}_{ss^*}(|\xi|)$ from now on. We introduce the symbol f to denote a nonnegative frequency, $f \geq 0$. The PSD matrix $\mathbf{P}_{ss^*}(f)$ can be written as

$$\mathbf{P}_{ss^*}(f) = \mathbf{T}\mathbf{P}_{zz}(f)\mathbf{T}^H \quad (17)$$

where

$$\mathbf{P}_{zz}(f) = \begin{bmatrix} P_{xx}(f) & P_{xy}(f) \\ P_{xy}^*(f) & P_{yy}(f) \end{bmatrix} \quad (18)$$

is the PSD matrix of $\mathbf{z}(t) = [x(t), y(t)]^T$. It contains the PSDs of $x(t)$ and $y(t)$, denoted by $P_{xx}(f)$ and $P_{yy}(f)$, and the cross-PSD of $x(t)$ and $y(t)$, denoted by $P_{xy}(f)$. It follows that we can express the PSD of $s(t)$ as

$$P_{ss^*}(f) = P_{xx}(f) + P_{yy}(f) + 2\text{Im}P_{xy}(f) \quad (19)$$

and the C-PSD of $s(t)$ as

$$P_{ss}(f) = P_{xx}(f) - P_{yy}(f) + 2j\text{Re}P_{xy}(f). \quad (20)$$

A proper process $s(t)$ has $P_{ss}(f) = 0$ and hence $P_{xx}(f) = P_{yy}(f)$ and $\text{Re}P_{xy}(f) = 0$. There is no condition on $\text{Im}P_{xy}(f)$ to ensure a proper $s(t)$. However, the PSD $P_{ss^*}(f)$ is even if and only if $\text{Im}P_{xy}(f) = 0$.

A linear filtering operation applied to the real and imaginary parts generally becomes *widely linear* [21], [24], or linear-conjugate linear [25] when applied to the complex signal. A stationary widely linear filtering operation depends linearly on $dS(f)$ and the conjugate $dS^*(-f)$

$$dZ(f) = H_1(f)dS(f) + H_2(f)dS^*(-f). \quad (21)$$

It is convenient to write this expression in an augmented notation

$$\begin{bmatrix} dZ(f) \\ dZ^*(-f) \end{bmatrix} = \begin{bmatrix} H_1(f) & H_2(f) \\ H_2^*(-f) & H_1^*(-f) \end{bmatrix} \begin{bmatrix} dS(f) \\ dS^*(-f) \end{bmatrix}. \quad (22)$$

It will be of interest to determine the eigenvalue decomposition of $\mathbf{P}_{ss^*}(f)$ for a fixed frequency f . Utilizing the representation (22) for widely linear transformations, such a decomposition is given by

$$\begin{bmatrix} P_{ss^*}(f) & P_{ss}(f) \\ P_{ss^*}^*(f) & P_{ss^*}(-f) \end{bmatrix} = \begin{bmatrix} G_1(f) & G_2(f) \\ G_2^*(-f) & G_1^*(-f) \end{bmatrix} \times \begin{bmatrix} \Lambda_1(f) & 0 \\ 0 & \Lambda_2(f) \end{bmatrix} \begin{bmatrix} G_1^*(f) & G_2(-f) \\ G_2^*(f) & G_1(-f) \end{bmatrix} \quad (23)$$

which we write in shorthand as

$$\mathbf{P}_{ss^*}(f) = \mathbf{G}(f)\mathbf{\Lambda}_{ss^*}(f)\mathbf{G}^H(f). \quad (24)$$

In this decomposition, $\Lambda_1(f)$ and $\Lambda_2(f)$, $\Lambda_1(f) \geq \Lambda_2(f)$, are the two eigenvalues of $\mathbf{P}_{ss^*}(f)$, and the matrix of eigenvectors $\mathbf{G}(f)$ is unitary, i.e.,

$$\mathbf{G}(f)\mathbf{G}^H(f) = \mathbf{I}. \quad (25)$$

Note that (24) describes a widely linear transformation, which depends on $dS(f)$ and $dS^*(-f)$.

We observe that $\Lambda_1(f) = \Lambda_2(f)$ requires that $s(t)$ be proper, $P_{ss}(f) = 0$, and the PSD be even, $P_{ss^*}(f) = P_{ss^*}(-f)$.

III. CHARACTERIZATION OF THE POLARIZATION ELLIPSE

We shall be interested in the path that the complex signal $s(t)$ describes in the complex plane. We will look at three cases, which are successively more general. In Section III-A, we begin with monochromatic deterministic signals. Section III-B looks at stationary, but not monochromatic, random signals, and Section IV finally considers the extension to nonstationary random signals. Section III-A and parts of Section III-B are required to establish ideas and notation. A presentation similar to that in Section III-A can also be found in [12].

A. Monochromatic Deterministic Signals

We start by considering the simplest case where $s(t)$ is *monochromatic* and *deterministic*. Its real and imaginary parts are then given by

$$\begin{cases} x(t) = A_x \cos(2\pi f_0 t + \phi_x) \\ y(t) = A_y \cos(2\pi f_0 t + \phi_y) \end{cases} \quad (26)$$

with nonnegative amplitudes A_x and A_y . It is easy to show [2] that $s(t)$ moves periodically around an ellipse as depicted in Fig. 1. Equation (26) is said to be a decomposition of this ellipse into linearly polarized components. In special cases, the ellipse degenerates to a circle or straight line. The ellipse parameters can be determined from the powers of and cross-power between the positive frequency components of the vector $\mathbf{z}(t) = [x(t), y(t)]^T$, as described by the so-called *coherency matrix* [2]

$$\mathbf{J}_{zz} = \frac{1}{4} \begin{bmatrix} A_x^2 & A_x A_y e^{j\phi} \\ A_x A_y e^{-j\phi} & A_y^2 \end{bmatrix} \quad (27)$$

with $\phi = \phi_x - \phi_y$.

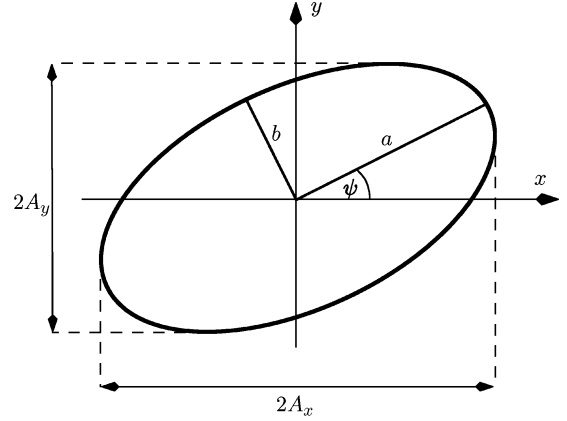


Fig. 1. Ellipse traced out by the monochromatic and deterministic signal $s(t)$ in the complex plane.

A complex representation equivalent to (26) is

$$s(t) = x(t) + jy(t) = \underbrace{A_+ e^{j\psi_+} e^{j2\pi f_0 t}}_{s_+(t)} + \underbrace{A_- e^{-j\psi_-} e^{-j2\pi f_0 t}}_{s_-(t)}. \quad (28)$$

This is the sum of a counterclockwise and clockwise rotating phasor, which are called the *rotary components* or *circularly polarized components*. The coherency matrix of the complex signal $s(t)$ contains the powers of and cross-power between the rotary components $[s_+(t), s_-^*(t)]^T$,

$$\begin{aligned} \mathbf{J}_{ss^*} &= \begin{bmatrix} |s_+(t)|^2 & s_+(t)s_-(t) \\ s_+^*(t)s_-^*(t) & |s_-(t)|^2 \end{bmatrix} \\ &= \begin{bmatrix} A_+^2 & A_+ A_- e^{j2\psi} \\ A_+ A_- e^{-j2\psi} & A_-^2 \end{bmatrix} \end{aligned} \quad (29)$$

with $2\psi = \psi_+ - \psi_-$. The discussion in [1], [2] is presented in terms of real and imaginary parts but we will see that the coherency matrix \mathbf{J}_{ss^*} of the complex signal $s(t)$ is a more natural and elegant way than \mathbf{J}_{zz} to describe the ellipse parameters. The two representations (26) and (28) are related through $\mathbf{J}_{ss^*} = \mathbf{T}\mathbf{J}_{zz}\mathbf{T}^H$, from which we determine the following useful expressions:

$$A_+^2 + A_-^2 = \frac{A_x^2 + A_y^2}{2} \quad (30)$$

$$A_+^2 - A_-^2 = A_x A_y \sin \phi \quad (31)$$

$$\tan 2\psi = \frac{2A_x A_y \cos \phi}{A_x^2 - A_y^2} = \frac{\text{Re}\{A_+ A_- e^{j2\psi}\}}{\text{Im}\{A_+ A_- e^{j2\psi}\}}. \quad (32)$$

The ellipse in Fig. 1 is inscribed in a rectangle whose sides are parallel to the x - and y -axes and have lengths $2A_x$ and $2A_y$. It can be shown [2] that the *orientation* of the ellipse, i.e., the angle between the major axis and the x -axis, is $\psi = (\psi_+ - \psi_-)/2$ as given by (32). We denote the lengths of the major and minor axes of the ellipse by $2a$ and $2b$, respectively. The area of the ellipse is

$$ab\pi = \pi A_x A_y |\sin \phi| = \pi |A_+^2 - A_-^2|, \quad (33)$$

and the numerical eccentricity is the ratio of geometric mean to arithmetic mean of A_+ and A_- ,

$$\frac{\sqrt{a^2 - b^2}}{a} = \frac{2\sqrt{A_+A_-}}{A_+ + A_-}. \quad (34)$$

We will further introduce another angle χ ($-\pi/4 \leq \chi \leq \pi/4$) as in [2]

$$\sin 2\chi = \frac{2A_xA_y \sin \phi}{A_x^2 + A_y^2} = \frac{A_+^2 - A_-^2}{A_+^2 + A_-^2} = \pm \frac{2ab}{a^2 + b^2} \quad (35)$$

and hence,

$$\tan \chi = \pm \frac{b}{a} \quad (36)$$

specifies the scale-invariant shape of the ellipse.

In (35) and (36), the sign on the right-hand side determines the turning direction of the ellipse. For $\sin \phi > 0$ and hence $0 < \chi \leq \pi/4$, $s(t)$ traces out the ellipse in *counterclockwise* direction, and for $\sin \phi < 0$ and thus $-\pi/4 \leq \chi < 0$, in *clockwise* direction. In these cases, $s(t)$ is called *counterclockwise* or *clockwise polarized*. In optics, counterclockwise (clockwise) polarization is also called *left-handed* (*right-handed*) polarization.

In special cases, the shape of the ellipse degenerates into a line or circle [2]. In *linear polarization*, the signal $s(t)$ describes a line. That means that $\sin \phi = 0$ and because of (31) and (35), $A_+ = A_-$ and thus $\chi = 0$. In *clockwise* (*right-handed*) *circular polarization*, $A_x = A_y$ and $\sin \phi = 1$, and because of (30) and (31), $A_+ = 0$ and thus $\chi = -\pi/4$. In *counterclockwise* (*left-handed*) *circular polarization*, $A_x = A_y$ and $\sin \phi = -1$, and thus, $A_- = 0$ and $\chi = \pi/4$.

B. Stationary Signals

We will now generalize the discussion to the case where $s(t)$ is a stationary random signal. We rewrite the spectral representation (3) as

$$s(t) = \int_0^{\infty} dS(f)e^{j2\pi ft} + dS(-f)e^{-j2\pi ft} \quad (37)$$

conforming to our convention that f denotes nonnegative frequencies.¹ This represents $s(t)$ as the superposition of ellipses, and one ellipse

$$u_f(t) = \underbrace{dS(f)e^{j2\pi ft}}_{u_{f+}(t)} + \underbrace{dS(-f)e^{-j2\pi ft}}_{u_{f-}(t)} \quad (38)$$

can be constructed for a given frequency $f \geq 0$. This point of view is common in oceanography [6], [7] but an alternative interpretation, which will prove to be more powerful, is the following. It can easily be shown that the random ellipse $u_f(t)$ is

¹This creates the minor technical issue that $dS(0)$ is counted twice in the integral (37). This is easily addressed by appropriate scaling of $dS(0)$ by a factor of $1/2$.

the *best linear approximation* of $s(t)$ from frequency components at $+f$ and $-f$. That is, the estimate $\hat{s}_f(t)$

$$\hat{s}_f(t) = H(f)dS(f)e^{j2\pi ft} + H(-f)dS(-f)e^{-j2\pi ft} \quad (39)$$

which linearly estimates $s(t)$ from the counterclockwise rotary component $u_{f+}(t)$ and the clockwise rotary component $u_{f-}(t)$ with minimum mean-squared error $E|s(t) - \hat{s}_f(t)|^2$, is indeed obtained for $H(f) = 1$ and $H(-f) = 1$. Hence, $\hat{s}_f(t) = u_f(t)$ as given by (38). Of course, $dS(f)$ and $dS(-f)$ are random variables, and so the ellipse $u_f(t)$ is random as well.

It is well known [25], [26] that *analytic* stationary signals are proper, $P_{ss}(f) = 0$. Thus, for analytic stationary signals, the linear estimate (39) cannot be improved upon by using a *widely linear* estimate. However, in the general nonanalytic case, $P_{ss}(f)$ is nonzero, and one may wonder if there exists a better widely linear estimate

$$\hat{s}_f^{WL}(t) = [H_1(f)dS(f) + H_2(f)dS^*(-f)]e^{j2\pi ft} + H_1(-f)dS(-f) + H_2(-f)dS^*(f)]e^{-j2\pi ft} \quad (40)$$

such that $E|s(t) - \hat{s}_f^{WL}(t)|^2 \leq E|s(t) - \hat{s}_f(t)|^2$. Yet it is again straightforward to show that such is not the case: The best widely linear estimator is indeed the linear estimator, $\hat{s}_f^{WL}(t) = \hat{s}_f(t)$. This means that even if $P_{ss}(f) \neq 0$, i.e., $dS(f)$ and $dS^*(-f)$ are correlated, it is not possible to exploit this correlation to achieve a smaller widely linear mean-squared approximation error. As we shall see in the next section, this result holds only in the stationary case and does not apply to nonstationary signals.

The statistical properties of the stationary random ellipse $u_f(t)$ are determined by the PSD matrix

$$\mathbf{P}_{ss^*}(f) = \begin{bmatrix} P_{ss^*}(f) & P_{ss}(f) \\ P_{ss}^*(f) & P_{ss^*}(-f) \end{bmatrix}. \quad (41)$$

The expected area of the ellipse is

$$\pi |P_{ss^*}(f) - P_{ss^*}(-f)| df \quad (42)$$

and the expected rotation direction of the ellipse is given by the sign of $P_{ss^*}(f) - P_{ss^*}(-f)$, where “+” indicates counterclockwise and “-” clockwise direction.

However, the phase of the C-PSD [7]

$$\tan 2\bar{\psi}(f) = \frac{\text{Im}P_{ss}(f)}{\text{Re}P_{ss}(f)} \quad (43)$$

only gives an *approximation* of the expected ellipse orientation. Similarly

$$\sin 2\bar{\chi}(f) = \frac{P_{ss^*}(f) - P_{ss^*}(-f)}{P_{ss^*}(f) + P_{ss^*}(-f)} \quad (44)$$

approximates the expected ellipse shape. The approximations (43) and (44) are obtained from (32) and (35), respectively, by applying the expectation operator to numerator and denominator separately, which ignores the fact that these are generally correlated, and exchanging the order of the expectation operator and the sin or tan function.

IV. POLARIZATION ELLIPSE OF NONSTATIONARY SIGNALS

The stationary ellipse $u_f(t)$ given by (38) is a *global* description and therefore inadequate to describe the time-varying characteristics of a *nonstationary* signal $s(t)$. In order to obtain a *local* description at time t and frequency f , we determine the widely linear minimum mean-squared error (WMMSE) approximation of $s(t)$ from frequency components at $+f$ and $-f$,

$$\hat{s}_f^{WL}(t) = \underbrace{[W_1(t, f)dS(f) + W_2(t, f)dS^*(-f)]}_{U(t, f)} e^{j2\pi ft} + \underbrace{[W_1(t, -f)dS(-f) + W_2(t, -f)dS^*(f)]}_{U(t, -f)} e^{-j2\pi ft}. \quad (45)$$

For fixed (t, f) but varying τ ,²

$$u_{t, f}(\tau) = \underbrace{U(t, f)e^{j2\pi f\tau}}_{u_{t, f_+}(\tau)} + \underbrace{U(t, -f)e^{-j2\pi f\tau}}_{u_{t, f_-}(\tau)} \quad (46)$$

describes an ellipse in the complex time-domain plane. Hence, τ traces out a “frozen” *local ellipse* $u_{t, f}(\tau)$ whose parameters are fixed for a given (t, f) . This local ellipse provides the best approximation of $s(t)$ at $\tau = t$. It is the sum of the rotary components $u_{t, f_+}(\tau)$ and $u_{t, f_-}(\tau)$. One ellipse can be constructed for every time-frequency pair (t, f) . Since (t, f) is fixed, $U(t, f)$ and $U(t, -f)$ are *random variables*. These will now play roles comparable to $dS(f)$ and $dS(-f)$ in the stationary ellipse (38).

A. Time-Varying Wiener Filter

We will now determine the optimum filter $W_1(t, \pm f)$ and $W_2(t, \pm f)$ in (45). With the short-hand notation

$$d\mathbf{Z}(t, f) = \begin{bmatrix} dS(f)e^{j2\pi ft} \\ dS^*(-f)e^{j2\pi ft} \\ dS(-f)e^{-j2\pi ft} \\ dS^*(f)e^{-j2\pi ft} \end{bmatrix} \quad (47)$$

the local ellipse is found as the output of a *time-varying Wiener (WMMSE) filter*

$$u_{t, f}(\tau)df = \mathbf{V}_{sZ^*}(t, f)\mathbf{K}_{ZZ^*}^\dagger(t, f)d\mathbf{Z}(\tau, f) \quad (48)$$

with

$$\begin{aligned} \mathbf{V}_{sZ^*}(t, f)df &= E [s(t)d\mathbf{Z}^H(t, f)] \\ &= \begin{bmatrix} V_{ss^*}(t, f) \\ V_{ss}(t, f) \\ V_{ss^*}(t, -f) \\ V_{ss}(t, -f) \end{bmatrix}^T df \end{aligned} \quad (49)$$

$$\mathbf{K}_{ZZ^*}(t, f)(df)^2 = E [d\mathbf{Z}(t, f)d\mathbf{Z}^H(t, f)]. \quad (50)$$

In (48), $(\cdot)^\dagger$ denotes the Moore–Penrose pseudoinverse (or generalized inverse), which is necessary because $\mathbf{K}_{ZZ^*}(t, f)$ can be singular. For a square full-rank matrix, the pseudoinverse is the standard matrix inverse.

This Wiener filter produces an ellipse $u_{t, f}(\tau)$ that, at $\tau = t$, is the WMMSE approximation of $s(t)$ from frequency components at $+f$ and $-f$. We again emphasize that t and f are fixed, and τ varies as it traces out the local ellipse. It is important to realize that the ellipse $u_{t, f}(\tau)$ is itself *nonstationary* because the random variable $U(t, f)$ generally has nonzero correlation with the random variable $U(t, -f)$, unlike the *stationary* case where $dS(f)$ is not correlated with $dS(-f)$.

The approximation error at time t is

$$E |s(t) - \hat{s}_f^{WL}(t)|^2 = r_{ss^*}(t, 0) - \mathbf{V}_{sZ^*}(t, f)\mathbf{K}_{ZZ^*}^\dagger(t, f) \times \mathbf{V}_{sZ^*}^H(t, f) \quad (51)$$

$$= r_{ss^*}(t, 0) (1 - |\rho(t, f)|^2) \quad (52)$$

where we have introduced the magnitude-squared *time-frequency coherence*

$$|\rho(t, f)|^2 = \frac{\mathbf{V}_{sZ^*}(t, f)\mathbf{K}_{ZZ^*}^\dagger(t, f)\mathbf{V}_{sZ^*}^H(t, f)}{r_{ss^*}(t, 0)}. \quad (53)$$

The magnitude-squared time-frequency coherence satisfies $0 \leq |\rho(t, f)|^2 \leq 1$. If $|\rho(t, f)|^2 = 1$, the ellipse $u_{t, f}(\tau)$ is a perfect approximation of $s(t)$ at time $\tau = t$. If $|\rho(t, f)|^2 = 0$, the best-fit ellipse $u_{t, f}(\tau)$ has vanishing amplitude.

A closed-form solution for the Wiener filter is tedious because it involves the pseudo-inverse of the 4×4 matrix $\mathbf{K}_{ZZ^*}(t, f)$. As shown in Fig. 2, this matrix contains ESDs and complementary ESDs in the northwest and southeast 2×2 blocks, and rotated Hermitian and complementary spectral correlations in the northeast and southwest 2×2 blocks. However, as illustrated in the figure, in special cases, $\mathbf{K}_{ZZ^*}(t, f)$ has many zero entries and the expression for the Wiener filter simplifies accordingly.

For instance, in the *stationary* case, $dS(f)$ and $dS^*(-f)$ are each uncorrelated with either $dS(-f)$ or $dS^*(f)$. Hence, $\mathbf{K}_{ZZ^*}(t, f)$ has zero northeast and southwest blocks, and computing the inverse of $\mathbf{K}_{ZZ^*}(t, f)$ amounts to computing the inverses of the northwest and southeast blocks. Using $P_{ss^{(*)}}(f) = V_{ss^{(*)}}(t, f) = R_{ss^{(*)}}(0, f)df$, it is then easy to show that $W_1(t, \pm f) = 1$ and $W_2(t, \pm f) = 0$, and (46) reduces to (38). This means that $u_{t, f}(t) = u_f(t)$ for *all* t , if $s(t)$ is stationary.

In order to characterize the expected properties of the random ellipse $u_{t, f}(\tau)$, we introduce the time- and frequency-dependent coherency matrix

$$\mathbf{J}_{uu^*}(t, f) = \begin{bmatrix} J_{uu^*}(t, f) & J_{uu}(t, f) \\ J_{uu^*}^*(t, f) & J_{uu^*}(t, -f) \end{bmatrix} \quad (54)$$

$$= E \begin{bmatrix} U(t, f) \\ U^*(t, -f) \end{bmatrix} [U^*(t, f) \quad U(t, -f)] \quad (55)$$

which contains the powers of and cross-power between the rotary components $[u_{t, f_+}(\tau), u_{t, f_-}^*(\tau)]^T$ in (46). The coherency matrix $\mathbf{J}_{uu^*}(t, f)$ mirrors the structure and plays a similar role as the PSD matrix $\mathbf{P}_{ss^*}(f)$ in the stationary case, and the coherency matrix \mathbf{J}_{ss^*} in the monochromatic deterministic case. Note that we do not study $\mathbf{J}_{uu}(t, f)$ as the ellipse parameters we are interested in are determined by $\mathbf{J}_{uu^*}(t, f)$. This, however,

²The time variable τ introduced here has no connection to τ in Section II.

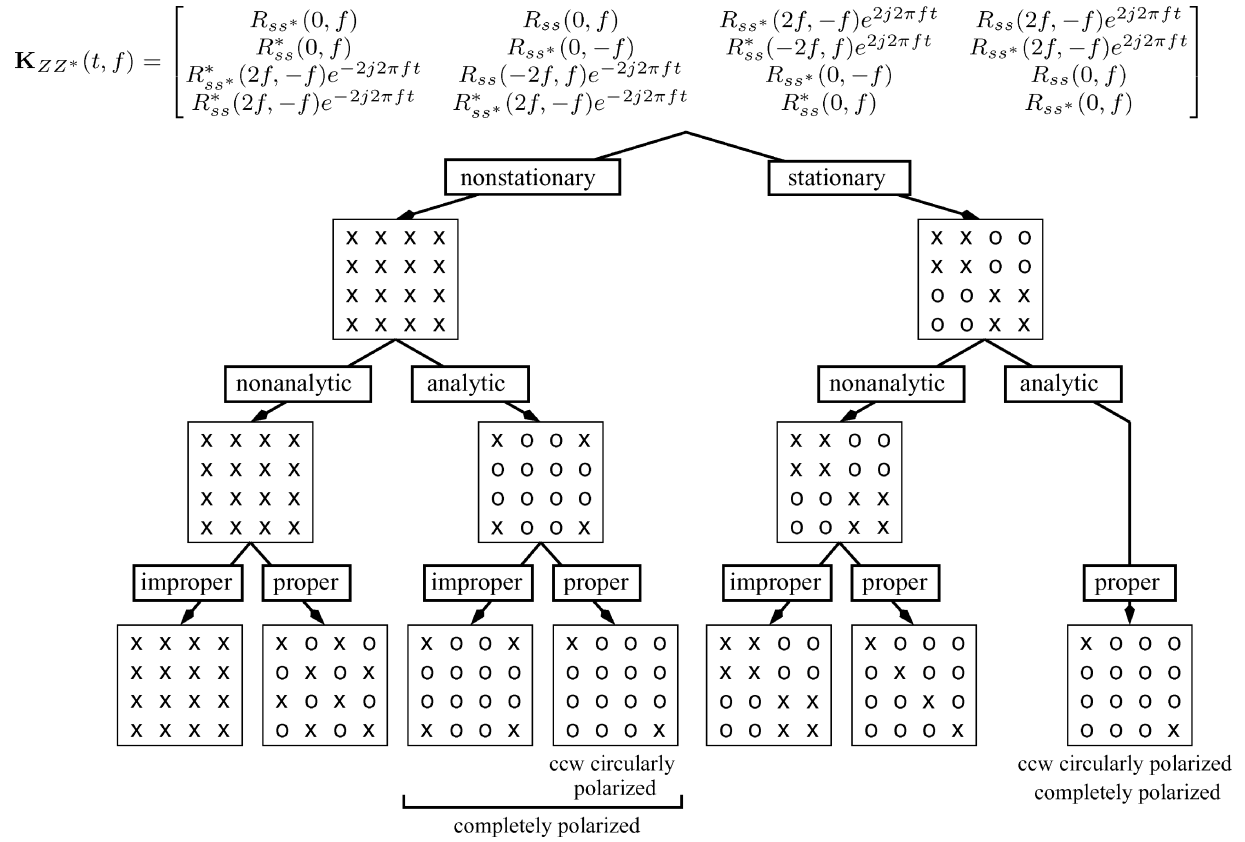


Fig. 2. This tree shows which entries of the 4×4 matrix $\mathbf{K}_{ZZ^*}(t, f)$ are generally nonzero (marked by x) and which entries must be zero (marked by o), for different properties of the signal $s(t)$.

leaves open the question whether or not $\mathbf{J}_{uu}(t, f)$ contains *any* interesting information.

The time- and frequency-dependent expected orientation of the ellipse is then approximated by

$$\tan 2\bar{\psi}(t, f) = \frac{\text{Im}J_{uu}(t, f)}{\text{Re}J_{uu}(t, f)}. \quad (56)$$

The expected area of the ellipse is

$$\pi |J_{uu^*}(t, f) - J_{uu^*}(t, -f)| \quad (57)$$

and its shape is approximately characterized by

$$\sin 2\bar{\chi}(t, f) = \frac{J_{uu^*}(t, f) - J_{uu^*}(t, -f)}{J_{uu^*}(t, f) + J_{uu^*}(t, -f)}. \quad (58)$$

B. Analytic Signals

For analytic signals (as well as anti-analytic signals), the expressions for $\bar{\psi}(t, f)$, $\bar{\chi}(t, f)$, and $|\rho(t, f)|^2$ simplify significantly. If $s(t)$ is analytic, $dS(-f) = 0$ and the ellipse (46) reduces to

$$u_{t,f}(\tau) = \underbrace{W_1(t, f)dS(f)}_{U(t, f)} e^{j2\pi f\tau} + \underbrace{W_2(t, -f)dS^*(f)}_{U(t, -f)} e^{-j2\pi f\tau}. \quad (59)$$

When determining the time-varying Wiener filter, we have to distinguish the two cases $(R_{ss^*}(0, f))^2 \neq |R_{ss}(2f, -f)|^2$

and $(R_{ss^*}(0, f))^2 = |R_{ss}(2f, -f)|^2$. In the latter situation, $dS^*(f) = \alpha dS(f)$, $|\alpha| = 1$, so that a widely linear estimator offers no advantage over a strictly linear estimator, that is, $W_2(t, -f) = 0$. From (48), the time-varying Wiener filter is found as

$$W_1(t, f)df = \begin{cases} \frac{V_{ss^*}R_{ss^*} - V_{ss}R_{ss}^*e^{-2j2\pi ft}}{(R_{ss^*}^2 - |R_{ss}|^2)}, & R_{ss^*}^2 \neq |R_{ss}|^2 \\ \frac{V_{ss^*}}{R_{ss^*}}, & R_{ss^*}^2 = |R_{ss}|^2 \end{cases} \quad (60)$$

$$W_2(t, -f)df = \begin{cases} \frac{V_{ss}R_{ss^*} - V_{ss^*}R_{ss}e^{2j2\pi ft}}{(R_{ss^*}^2 - |R_{ss}|^2)}, & R_{ss^*}^2 \neq |R_{ss}|^2 \\ 0, & R_{ss^*}^2 = |R_{ss}|^2. \end{cases} \quad (61)$$

For notational convenience, we have dropped the function arguments in these two equations. It is understood that V_{ss^*} stands for $V_{ss^*}(t, f)$, V_{ss} for $V_{ss}(t, -f)$, R_{ss^*} for $R_{ss^*}(0, f)$, and R_{ss} for $R_{ss}(2f, -f)$. The time- and frequency-dependent coherency matrix $\mathbf{J}_{uu^*}(t, f)$ can now be evaluated as

$$\mathbf{J}_{uu^*}(t, f) = E \begin{bmatrix} W_1(t, f)dS(f) \\ W_2^*(t, -f)dS(f) \end{bmatrix} \begin{bmatrix} W_1^*(t, f)dS^*(f) \\ W_2(t, -f)dS^*(f) \end{bmatrix}^T \\ = R_{ss^*}(0, f)(df)^2 \\ \times \begin{bmatrix} |W_1(t, f)|^2 & W_1(t, f)W_2(t, -f) \\ W_1^*(t, f)W_2^*(t, -f) & |W_2(t, -f)|^2 \end{bmatrix}. \quad (62)$$

It is particularly interesting to examine the ellipse shape and polarization, which, for $R_{ss^*}^2 \neq |R_{ss}|^2$, can be done through the angle

$$\begin{aligned} \sin 2\bar{\chi}(t, f) &= \frac{N}{D} \\ N &= (|V_{ss^*}|^2 - |V_{ss}|^2) (R_{ss^*}^2 - |R_{ss}|^2) \\ D &= (|V_{ss^*}|^2 + |V_{ss}|^2) (R_{ss^*}^2 + |R_{ss}|^2) \\ &\quad - 4\text{Re} \{V_{ss^*} V_{ss}^* R_{ss^*} R_{ss} e^{2j2\pi ft}\}. \end{aligned} \quad (63)$$

If $s(t)$ is proper at time t and frequency f , $V_{ss} = 0$ and $R_{ss} = 0$, then $\bar{\chi}(t, f) = \pi/4$. This says that a proper analytic signal is *counterclockwise circularly polarized*. On the other hand, if $R_{ss^*}^2 = |R_{ss}|^2$, then $dS^*(f) = \alpha dS(f)$, $|\alpha| = 1$, and it follows that $|V_{ss^*}|^2 = |V_{ss}|^2$. In this case, the signal $s(t)$ can be regarded as maximally improper at frequency f . A maximally improper analytic signal has $\bar{\chi}(t, f) = \pi/4$ and is therefore also *counterclockwise circularly polarized*.

While $|R_{ss}|^2 \leq R_{ss^*}^2$, the magnitude of the HR-TFD does not provide an upper bound on the magnitude of the CR-TFD, i.e., $|V_{ss}|^2 \not\leq |V_{ss^*}|^2$. Moreover, $|V_{ss^*}|^2 = |V_{ss}|^2$ does not imply $R_{ss^*}^2 = |R_{ss}|^2$. Therefore, *it is possible that $s(t)$ is clockwise polarized at (t, f)* , i.e., $\bar{\chi}(t, f) < 0$, provided that the signal is “sufficiently improper” at (t, f) . This result may seem surprising, considering that an analytic signal is synthesized from *counterclockwise* phasors only.

The quality of the approximation can be judged by computing the magnitude-squared time-frequency coherence $|\rho(t, f)|^2$, for which we obtain

$$\begin{aligned} |\rho(t, f)|^2 &= \frac{R_{ss^*} (|V_{ss^*}|^2 + |V_{ss}|^2) - 2\text{Re} \{V_{ss^*} V_{ss}^* R_{ss^*} e^{2j2\pi ft}\}}{r_{ss^*}(t, 0) (R_{ss^*}^2 - |R_{ss}|^2)} \end{aligned} \quad (64)$$

if $R_{ss^*}^2 \neq |R_{ss}|^2$. In both the proper case, which is characterized by $V_{ss} = 0$ and $R_{ss} = 0$, and the most improper case, characterized by $R_{ss^*}^2 = |R_{ss}|^2$, the magnitude-squared time-frequency coherence becomes [19]

$$|\rho(t, f)|^2 = \frac{|V_{ss^*}(t, f)|^2}{r_{ss^*}(t, 0) R_{ss^*}^2(0, f)} \quad (65)$$

because in these cases $s(t)$ can be estimated from counterclockwise rotating phasors only. In other words, the optimum widely linear estimator is strictly linear, which means $W_2(t, -f) = 0$ in (59).

The expression (64), a special case of (53), was derived by [27] as the time-frequency coherence of a generally *nonanalytic* signal because [27] did not combine contributions from positive and negative frequency components. This amounts to estimating $s(t)$ from $dS(f)e^{j2\pi ft}$ and $dS^*(f)e^{-j2\pi ft}$, but *separately* for positive and negative frequencies. Hence, [27] defined (64) separately for positive and negative frequencies, with generally different values at $+f$ and $-f$. Moreover, if positive and negative frequency contributions are not combined, (65) is the time-frequency coherence for *analytic improper* signals for $f > 0$, as shown by [19].

V. POLARIZATION ANALYSIS

We call a nonstationary random signal $s(t)$ *completely polarized* at (t, f) if the corresponding local ellipse $u_{t,f}(\tau)$ given by (46) has complete coherence between counterclockwise and clockwise rotating phasors, i.e.,

$$U(t, f) = cU^*(t, -f) \quad (66)$$

for some complex *constant* c , or equivalently,

$$|J_{uu}(t, f)|^2 = J_{uu^*}(t, f)J_{uu^*}(t, -f). \quad (67)$$

The condition (67) is equivalent to $\det \mathbf{J}_{uu^*}(t, f) = 0$, which means that $\mathbf{J}_{uu^*}(t, f)$ has one nonzero and one zero eigenvalue.

We should point out that a signal that is completely polarized in the sense of (66) does *not* have to be polarized in the sense that the *shape* of the ellipse degenerates into a line or circle, which is called linear or circular polarization. On the other hand, a linearly or circularly polarized signal does not have to be completely polarized in the sense of (66) either. “Shape polarization,” as discussed in Section III-A, is not the subject of this section.

In this section, we extend polarization analysis to nonstationary random signals, following ideas from [1], [2]. The development is based on the time- and frequency-dependent coherency matrix $\mathbf{J}_{uu^*}(t, f)$. However, it can easily be applied to stationary signals as well, using the time-independent PSD matrix $\mathbf{P}_{ss^*}(f)$ in place of $\mathbf{J}_{uu^*}(t, f)$.

A. Degree of Polarization

In analogy to the definition for partially polarized light [1], [2], we now define the degree of polarization $\Phi(t, f)$ as the ratio of the time-averaged³ polarized power to the time-averaged total power of the ellipse $u_{t,f}(\tau)$ at given (t, f) ,

$$\Phi(t, f) = \frac{P_{\text{pol}}(t, f)}{P_{\text{tot}}(t, f)}. \quad (68)$$

This requires that we decompose the coherency matrix $\mathbf{J}_{uu^*}(t, f)$ into two parts

$$\mathbf{J}_{uu^*}(t, f) = \mathbf{J}_{pp^*}(t, f) + \mathbf{J}_{\overline{pp}^*}(t, f) \quad (69)$$

where $\mathbf{J}_{pp^*}(t, f)$ represents the coherency matrix of the completely polarized component and $\mathbf{J}_{\overline{pp}^*}(t, f)$ the coherency matrix of the unpolarized component. Starting with the eigenvalue decomposition of $\mathbf{J}_{uu^*}(t, f)$, which is obtained analogously to (24) at fixed (t, f) ,

$$\mathbf{J}_{uu^*}(t, f) = \mathbf{G}(t, f)\mathbf{\Lambda}_{uu^*}(t, f)\mathbf{G}^H(t, f) \quad (70)$$

we decompose $\mathbf{\Lambda}_{uu^*}(t, f)$ as [2]

$$\mathbf{\Lambda}_{uu^*}(t, f) = \mathbf{\Lambda}_{pp^*}(t, f) + \mathbf{\Lambda}_{\overline{pp}^*}(t, f) \quad (71)$$

$$\mathbf{\Lambda}_{pp^*}(t, f) = \begin{bmatrix} \Lambda_1(t, f) & -\Lambda_2(t, f) & 0 \\ 0 & \Lambda_2(t, f) & 0 \end{bmatrix} \quad (72)$$

$$\mathbf{\Lambda}_{\overline{pp}^*}(t, f) = \begin{bmatrix} \Lambda_2(t, f) & 0 \\ 0 & \Lambda_2(t, f) \end{bmatrix} \quad (73)$$

³The time averaging is performed with respect to τ , not t . This time averaging is necessary because the ellipse $u_{t,f}(\tau)$ is nonstationary.

and synthesize $\mathbf{J}_{pp^*}(t, f)$ and $\mathbf{J}_{\overline{pp}^*}(t, f)$ as

$$\mathbf{J}_{pp^*}(t, f) = \mathbf{G}(t, f)\mathbf{\Lambda}_{pp^*}(t, f)\mathbf{G}^H(t, f) \quad (74)$$

$$\mathbf{J}_{\overline{pp}^*}(t, f) = \mathbf{G}(t, f)\mathbf{\Lambda}_{\overline{pp}^*}(t, f)\mathbf{G}^H(t, f). \quad (75)$$

The degree of polarization at (t, f) is thus found as

$$\Phi(t, f) = \frac{\Lambda_1(t, f) - \Lambda_2(t, f)}{\Lambda_1(t, f) + \Lambda_2(t, f)} \quad (76)$$

which can be evaluated by using an explicit expression for the two eigenvalues of the 2×2 coherency matrix $\mathbf{J}_{uu^*}(t, f)$. We obtain, in analogy to the solution for partially polarized light [1], [2]

$$\Phi(t, f) = \sqrt{1 - \frac{4 \det \mathbf{J}_{uu^*}(t, f)}{\text{tr}^2 \mathbf{J}_{uu^*}(t, f)}} \quad (77)$$

where $\text{tr}(\cdot)$ denotes the trace of a matrix.

The degree of polarization satisfies $0 \leq \Phi(t, f) \leq 1$. When $\Phi(t, f) = 1$, then $\Lambda_2(t, f) = 0$, $\det \mathbf{J}_{uu^*}(t, f) = 0$, and $s(t)$ is completely polarized at (t, f) . In that case, *all* sample functions of the local ellipse $u_{t,f}(\tau)$ trace out the ellipse in the same direction, which is either clockwise (if $-\pi/4 \leq \bar{\chi}(t, f) < 0$) or counterclockwise (if $0 < \bar{\chi}(t, f) \leq \pi/4$). Monochromatic deterministic signals are always completely polarized, which can be seen from $\det \mathbf{J}_{ss^*} = 0$ for the coherency matrix given by (29). Moreover, all analytic signals are completely polarized for all (t, f) , as is evident from $\det \mathbf{J}_{uu^*}(t, f) = 0$ for the coherency matrix given by (62). Completely polarized signals are called *degenerate* in [21].

When $\Phi(t, f) = 0$, then $\Lambda_1(t, f) = \Lambda_2(t, f)$, $J_{uu^*}(t, f) = J_{uu^*}(t, -f)$, and $U(t, f)$ and $U^*(t, -f)$ from (46) are uncorrelated, $J_{uu}(t, f) = 0$. Obviously, $J_{uu}(t, f) = 0$ is only a necessary but not sufficient condition for $\Phi(t, f) = 0$. In fact, if $U(t, f)$ and $U^*(t, -f)$ are uncorrelated, the degree of polarization takes on a particularly simple form [2]

$$\Phi(t, f) = \left| \frac{J_{uu^*}(t, f) - J_{uu^*}(t, -f)}{J_{uu^*}(t, f) + J_{uu^*}(t, -f)} \right| \quad (78)$$

$$= |\sin 2\bar{\chi}(t, f)|. \quad (79)$$

The additional condition of $J_{uu^*}(t, f) = J_{uu^*}(t, -f)$ for a signal to be unpolarized at (t, f) can thus be visualized as a requirement that the local ellipse $u_{t,f}(\tau)$ have no preferred expected rotation direction.

B. Stokes Parameters

Stokes [3] introduced a set of four parameters to characterize the state of polarization of partially polarized light. These parameters have an interesting connection with the complex description we use in this paper. Here, we consider time- and frequency-dependent versions of the Stokes parameters. For notational convenience, however, we will drop the explicit time-frequency dependence of parameters in this section.

In terms of the real part $x(t)$ and the imaginary part $y(t)$, the Stokes parameters are defined as [2] $\Sigma_0 = J_{xx} + J_{yy}$, $\Sigma_1 =$

$J_{xx} - J_{yy}$, $\Sigma_2 = 2\text{Re}J_{xy}$, and $\Sigma_3 = 2\text{Im}J_{xy}$. The connection $\mathbf{J}_{uu^*} = \mathbf{T}\mathbf{J}_{zz}\mathbf{T}^H$ yields

$$\Sigma_0 = \text{Ev}J_{uu^*} = \frac{J_{uu^*}(t, f) + J_{uu^*}(t, -f)}{2} \quad (80)$$

$$\Sigma_1 = \text{Re}J_{uu} \quad (81)$$

$$\Sigma_2 = \text{Im}J_{uu} \quad (82)$$

$$\Sigma_3 = \text{Od}J_{uu^*} = \frac{J_{uu^*}(t, f) - J_{uu^*}(t, -f)}{2} \quad (83)$$

where $\text{Ev}J_{uu^*}$ and $\text{Od}J_{uu^*}$ denote the even and odd parts of J_{uu^*} with respect to f . The polarized power is [2]

$$P_{\text{pol}} = \sqrt{\Sigma_1^2 + \Sigma_2^2 + \Sigma_3^2} \quad (84)$$

$$= \sqrt{|J_{uu}|^2 + (\text{Od}J_{uu^*})^2} \quad (85)$$

and the total power is

$$P_{\text{tot}} = \Sigma_0 = \text{Ev}J_{uu^*}. \quad (86)$$

The degree of polarization (77) can thus be expressed as

$$\Phi = \frac{\sqrt{|J_{uu}|^2 + (\text{Od}J_{uu^*})^2}}{\text{Ev}J_{uu^*}}. \quad (87)$$

A completely polarized signal has $\Sigma_1^2 + \Sigma_2^2 + \Sigma_3^2 = \Sigma_0^2$, whereas an unpolarized signal has $\Sigma_1 = \Sigma_2 = \Sigma_3 = 0$ [2]. This fact makes the decomposition of the coherency matrix of a given signal into completely polarized and unpolarized part particularly simple. The coherency matrix of the polarized part is

$$\mathbf{J}_{pp^*} = \begin{bmatrix} P_{\text{pol}} + \Sigma_3 & \Sigma_1 + j\Sigma_2 \\ \Sigma_1 - j\Sigma_2 & P_{\text{pol}} - \Sigma_3 \end{bmatrix} \quad (88)$$

and the coherency matrix of the unpolarized part is

$$\mathbf{J}_{\overline{pp}^*} = \begin{bmatrix} P_{\text{tot}} - P_{\text{pol}} & 0 \\ 0 & P_{\text{tot}} - P_{\text{pol}} \end{bmatrix}. \quad (89)$$

VI. DISCUSSION AND CONCLUSION

In this paper, we have presented an extension of polarization and rotary-spectrum analysis to nonstationary random signals. Our extension seems natural if we take the point of view that polarization and rotary-spectrum analysis are about estimating a signal in the time domain from its frequency-domain description. At every point (t, f) in the time-frequency plane, we can construct a local ellipse that is the best widely linear approximation of the signal at time t from frequency components at $+f$ and $-f$. This ellipse is characterized by its time-dependent shape, orientation, and degree of polarization. We have defined a time-frequency coherence that determines how well the local ellipse at (t, f) approximates the signal at time t . In the analysis of a nonstationary signal $s(t)$, we should then focus on points (t, f) with magnitude-squared coherence close to 1.

The ellipse parameters and the time-frequency coherence can all be expressed in terms of the R-TFD, but both the HR-TFD and the CR-TFD are required. The CR-TFD is also necessary when analyzing a real signal via its corresponding analytic signal. Even though the corresponding analytic signal

is always completely polarized, shape, orientation, and rotation direction of the ellipse depend on the CR-TFD. Ignorance of the CR-TFD would seem to imply that all analytic signals are counterclockwise circularly polarized. This is true if the analytic signal is either proper or maximally improper. Otherwise, the polarization ellipse may not be a circle and may even (at least temporarily) turn clockwise.

The analysis in this paper has been presented based on the Hermitian and complementary correlations of the complex signal rather than the correlations and cross-correlations for real and imaginary parts. The main advantage is the behavior of these correlations under coordinate rotation, when $s(t)$ is replaced with $e^{j\phi}s(t)$ for a fixed real angle ϕ . In particular, the power of the rotary components and the cross-power between the rotary components of the local ellipse transform as

$$\begin{aligned} J_{uu^*} &\longrightarrow J_{uu^*} \\ J_{uu} &\longrightarrow e^{j2\phi} J_{uu} \end{aligned}$$

respectively. That is, J_{uu^*} and the magnitude of J_{uu} are invariant under coordinate rotation. It follows that the ellipse shape $\bar{\chi}$, degree of polarization Φ , and magnitude-squared time-frequency coherence $|\rho|^2$ are all *invariant* under coordinate rotation. On the other hand, the ellipse orientation $\bar{\psi}$ is *covariant* under coordinate rotation, i.e., it transforms as $\bar{\psi} \longrightarrow e^{j\phi}\bar{\psi}$.

Finally, it should be pointed out that a mathematically rigorous treatment would need to utilize measure theory. In order to make this paper as accessible as possible, this has been avoided. Unfortunately, in some instances, this leads to expressions that some readers may consider imprecise. However, rewriting this paper with complete mathematical rigor would not change any of the fundamental messages or results presented.

ACKNOWLEDGMENT

The author would like to thank Prof. L. Scharf for stimulating discussions and a critical reading of the manuscript, and three anonymous reviewers for many helpful comments and suggestions.

REFERENCES

- [1] E. Wolf, "Coherence properties of partially polarized electromagnetic radiation," *Nuovo Cimento*, vol. 13, pp. 1165–1181, 1959.
- [2] M. Born and E. Wolf, *Principles of Optics*. Cambridge, U.K.: Cambridge Univ. Press, 1999.
- [3] G. G. Stokes, "On the composition and resolution of streams of polarized light from different sources," *Trans. Camb. Phil. Soc.*, vol. 9, pp. 399–423, 1852.
- [4] A. G. Jones, "On the difference between polarisation and coherence," *J. Geophys.*, vol. 45, pp. 223–229, 1979.
- [5] J. C. Samson, "Comments on polarization and coherence," *J. Geophys.*, vol. 48, pp. 195–198, 1980.
- [6] J. Gonella, "A rotary-component method for analysing meteorological and oceanographic vector time series," *Deep-Sea Res.*, vol. 19, pp. 833–846, 1972.
- [7] C. N. K. Mooers, "A technique for the cross spectrum analysis of pairs of complex-valued time series, with emphasis on properties of polarized components and rotational invariants," *Deep-Sea Res.*, vol. 20, pp. 1129–1141, 1973.

- [8] J. Calman, "On the interpretation of ocean current spectra," *J. Phys. Oceanogr.*, vol. 8, pp. 627–652, 1978.
- [9] W. L. Stutzman, *Polarization in Electromagnetic Systems*. Norwood, MA: Artech House, 1992.
- [10] M. Loève, *Probability Theory*, 3rd ed. Princeton, NJ: Van Nostrand, 1963.
- [11] J. M. Lilly and J. Park, "Multiwavelet spectral and polarization analysis," *Geophys. J. Int.*, vol. 122, pp. 1001–1021, 1995.
- [12] J. M. Lilly and J.-C. Gascard, "Wavelet ridge diagnosis of time-varying elliptical signals with application to an oceanic eddy," *Nonlin. Processes Geophys.*, vol. 13, pp. 467–483, 2006.
- [13] S. Olhede and A. T. Walden, "Polarization phase relationships via multiple Morse wavelets. I. Fundamentals," *Proc. Roy. Soc. London A, Mat.*, vol. 459, pp. 413–444, 2003.
- [14] S. Olhede and A. T. Walden, "Polarization phase relationships via multiple Morse wavelets. II. Data analysis," *Proc. Roy. Soc. London A, Mat.*, vol. 459, pp. 641–657, 2003.
- [15] A. Roueff, J. Chanussot, and J. I. Mars, "Estimation of polarization parameters using time-frequency representations and its application to waves separation," *Signal Process.*, vol. 86, no. 12, pp. 3714–3731, Dec. 2006.
- [16] N. Delprat, B. Escudie, P. Guillemain, R. Kronland-Martinet, P. Tchamitchian, and B. Torresani, "Asymptotic wavelet and Gabor analysis: Extraction of instantaneous frequencies," *IEEE Trans. Inf. Theory*, vol. 38, no. 2, pp. 644–664, Mar. 1992.
- [17] A. W. Rihaczek, "Signal energy distribution in time and frequency," *IEEE Trans. Inf. Theory*, vol. 14, pp. 369–374, 1968.
- [18] L. Cohen, "Generalized phase-space distribution functions," *J. Math. Phys.*, vol. 7, no. 5, pp. 781–786, May 1966.
- [19] L. L. Scharf, P. J. Schreier, and A. Hanssen, "The Hilbert space geometry of the Rihaczek distribution for stochastic analytic signals," *IEEE Signal Process. Lett.*, vol. 12, no. 4, pp. 297–300, Apr. 2005.
- [20] P. J. Schreier, "A new interpretation of bilinear time-frequency distributions," in *Proc. Int. Conf. Acoustics, Speech, Signal Processing (ICASSP)*, Honolulu, HI, Apr. 2007, pp. III-1133–III-1136.
- [21] P. J. Schreier and L. L. Scharf, "Second-order analysis of improper complex random vectors and processes," *IEEE Trans. Signal Process.*, vol. 51, no. 3, pp. 714–725, Mar. 2003.
- [22] P. J. Schreier and L. L. Scharf, "Stochastic time-frequency analysis using the analytic signal: Why the complementary distribution matters," *IEEE Trans. Signal Process.*, vol. 51, no. 12, pp. 3071–3079, Dec. 2003.
- [23] P. Flandrin, *Time-Frequency/Time-Scale Analysis*. San Diego, CA: Academic, 1999.
- [24] B. Picinbono and P. Chevalier, "Widely linear estimation with complex data," *IEEE Trans. Signal Process.*, vol. 43, no. 8, pp. 2030–2033, Aug. 1995.
- [25] W. M. Brown and R. B. Crane, "Conjugate linear filtering," *IEEE Trans. Inf. Theory*, vol. 15, no. 4, pp. 462–465, Jul. 1969.
- [26] B. Picinbono and P. Bondon, "Second-order statistics of complex signals," *IEEE Trans. Signal Process.*, vol. 45, no. 2, pp. 411–419, Feb. 1997.
- [27] H. Hindberg and A. Hanssen, "Generalized spectral coherences for complex-valued harmonizable processes," *IEEE Trans. Signal Process.*, vol. 55, no. 6, pt. 1, pp. 2407–2413, Jun. 2007.



Peter J. Schreier (S'03–M'04) was born in Munich, Germany, in 1975. He received the M.S. degree from the University of Notre Dame, Notre Dame, IN, in 1999, and the Ph.D. degree from the University of Colorado at Boulder in 2003, both in electrical engineering.

In fall 1998, he was a visiting research student at the University of Hawaii at Manoa. From April 1999 to July 2000, he was with the Research Center 3-D Image Analysis and Synthesis at Friedrich-Alexander Universität Erlangen-Nürnberg, Germany. In spring 2004, he was a Postdoctoral Research Associate, and in spring 2008 a Visiting Associate Professor with Colorado State University, Ft. Collins. Since July 2004, he has been with the School of Electrical Engineering and Computer Science at The University of Newcastle, Australia, currently as a Senior Lecturer. His current research interests lie in the areas of statistical signal processing.